Mechanical and thermal behaviour of isotactic polypropylene reinforced with inorganic fullerene-like WS_2 nanoparticles: Effect of filler loading and temperature

Ana M. Díez-Pascual [a], Mohammed Naffakh [b,*]

[a] Instituto de Ciencia y Tecnología de Polímeros (ICTP-CSIC), Juan de la Cierva 3, 28006 Madrid, Spain
[b] Universidad Politécnica de Madrid, Departamento de Ingeniería y Ciencia de los Materiales, Escuela Técnica Superior de Ingenieros Industriales, José Gutiérrez Abascal 2, 28006 Madrid, Spain

HIGHLIGHTS

- The thermal and mechanical behaviour of iPP/IF-WS_2 nanocomposites was studied.
- Low IF-WS_2 contents provide a good balance between stiffness, strength and toughness.
- Their tensile behaviour is sensitive to the strain rate and temperature.
- The nanocomposites exhibit superior thermal conductivity and flame retardancy than iPP.
- The benefits of using IF-WS_2 compared to other nanoscale fillers are highlighted.

GRAPHICAL ABSTRACT

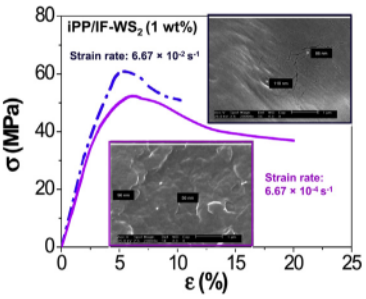

ABSTRACT

The thermal and mechanical behaviour of isotactic polypropylene (iPP) nanocomposites reinforced with different loadings of inorganic fullerene-like tungsten disulfide (IF-WS_2) nanoparticles was investigated. The IF-WS_2 noticeably enhanced the polymer stiffness and strength, ascribed to their uniform dispersion, the formation of a large nanoparticle–matrix interface combined with a nucleating effect on iPP crystallization. Their reinforcement effect was more pronounced at high temperatures. However, a drop in ductility and toughness was found at higher IF-WS_2 concentrations. The tensile behaviour of the nanocomposites was extremely sensitive to the strain rate and temperature, and their yield strength was properly described by the Eyring's equation. The activation energy increased while the activation volume decreased with increasing nanoparticle loading, indicating a reduction in polymer chain motion. The nanoparticles improved the thermomechanical properties of iPP: raised the glass transition and heat deflection temperatures while decreased the coefficient of thermal expansion. The nanocomposites also displayed superior flame retardancy with longer ignition time and reduced peak heat release rate. Further, a gradual rise in thermal conductivity was found with increasing IF-WS_2 loading both in the glassy and rubbery states. The results presented herein highlight the benefits and high potential of using IF-nanoparticles for enhancing the thermomechanical properties of thermoplastic polymers compared to other nanoscale fillers.

Keywords:
Composite materials
Tension test
Thermal conductivity
Thermomechanical effects

* Corresponding author. Tel.: +34 913363007; fax: +34 913363164.
E-mail address: mohammed.naffakh@upm.es (M. Naffakh).

1. Introduction

Polypropylene (PP) is a semicrystalline commodity plastic widely used in food packaging, medical care, automobile and other industrial sectors due to its low cost, easy processability, low density and well-balanced physical and mechanical properties like ductility and strength at room temperature and/or under moderate rates of deformation [1]. Nevertheless, under severe conditions it becomes brittle. A wide number of microfillers including mica, silica, alumina, talc, glass fibre, carbon black, etc [2–4] have been incorporated into PP to further improve its mechanical properties and simultaneously increase its longevity and durability, thus fulfilling the requirements for certain engineering applications. However, large amounts of these microfillers (20–30 wt%) are required to attain significant property enhancements, which has detrimental effects on the processability of the composites, increases cost and weight.

On the other hand, nanoparticle reinforced polymers are attracting a lot of attention in recent years due to their unique properties resulting from the nanoscale structures. The exceptionally high nanoparticle specific surface area enables the formation of a large interphase in the nanocomposite and strong nanofiller–matrix interactions. Thus, the addition of nanometric fillers such as montmorillonite clays [5], $CaCO_3$ [6], SiO_2 [7], carbon nitrides [8], or carbon nanotubes (CNTs) [9,10] to PP has been reported to improve significantly the Young's modulus and yield stress. For example, the incorporation of very low loadings (0.25 wt%) of single-walled carbon nanotubes (SWCNTs) led to a remarkable increase in stiffness and strength, by ca. 20%, albeit these properties were found to decrease at higher concentrations due to the formation of SWCNT aggregates. Therefore, a lot of effort is now focused on the design of novel strategies to prepare nanocomposites with optimal nanofiller dispersion. Amongst the most promising types of nanoreinforcements are inorganic nanoparticles of layered metal dichalcogenides such as WS_2 and MoS_2 [11] that possess similar structure to fullerenes. These non-carbon materials are named as inorganic fullerene-like (IF) nanoparticles and exhibit outstanding properties like very high stiffness and strength [12]; they are strong enough to withstand uniform pressures up to 21 GPa. This superior mechanical performance is ascribed to their small size (typically in the range of 40–180 nm), quasi-spherical shape, closed-cage layered structure and chemical inertness. Moreover, they are cheaper than organic nanofillers (i.e. CNTs, nanofibers, graphene), more environmentally friendly and display lower agglomerating tendency, hence can be homogenously dispersed within polymer matrices without the aid of surfactants or compatibilizing agents [13,14]. Further, the IF nanoparticles have excellent solid lubricant behaviour, and their efficiency as lubricant additives for improving the tribological properties of epoxy [15] and thermoplastic polymers [16,17] has been recently demonstrated.

Polymer matrix composites (PMCs) are commonly used in a wide variety of engineering applications such as aircraft, automotive and construction components, in which they are frequently subjected to different temperatures and dynamic loadings. In order to avoid any mishap during service, it is crucial to investigate the deformation behaviour of PMCs over a range of strain rates and temperatures, analyzing the influence of parameters such as filler size, quantity, shape and geometry as well as the interactions between fillers and matrix that play a major role in determining the overall mechanical performance. Previous works on strain rate deformation behaviour have primarily focused on neat polymers [18,19] and their microcomposites [20,21]. However, there exists little information available regarding the effects of temperature and deformation rate on the yield strength of thermoplastic based nanocomposites [22], particularly those reinforced with inorganic nanoparticles [23]. Thus, this is a great opportunity to ascertain the capabilities and possibilities of nanocomposites to replace conventional materials, especially in high temperature/strain rate applications.

In a previous work [14], isotactic polypropylene (iPP)/IF-WS_2 nanocomposites with various nanofiller loadings were prepared via traditional melt-blending process, and the experimental data demonstrated a remarkable enhancement in the thermal stability as well as an increase in the crystallization rate of the matrix when compared with neat iPP. The aim of the current study is to show the advantages of using IF nanoparticles as a suitable alternative for other inorganic and organic nanofillers that have been used for enhancing the mechanical and thermal properties of PP. To achieve this goal, the effect of IF-WS_2 content, strain rate and temperature on the Young's modulus, yield strength, tensile elongation and toughness of this thermoplastic matrix has been explored in detail, and the results have been compared to those reported for iPP/CNT and iPP/SiO_2 nanocomposites. Further, the influence of the IF nanoparticles on different thermomechanical properties including the coefficient of thermal expansion (CTE), heat deflection temperature (HDT) and glass transition temperature (T_g) as well as on the thermal behaviour like flammability and thermal conductivity is analyzed.

2. Experimental section

2.1. Materials and processing

iPP was supplied by Repsol-YPF (Spain), with 95% isotacticity, a viscosity average molecular weight of 179,000 g mol^{-1} and a polydispersity of 4.77. Inorganic fullerene-like tungsten disulfide (IF-WS_2) nanoparticles (NanoLub™, $d_{25°C}$ ~7.5 g cm^{-3}) were provided by Nanomaterials (Israel). A detailed morphological study of these nanomaterials using SEM was carried out in the preceding work [14]. They are closed-cage hollow multilayered polyhedral nanoparticles with a shape ranging from spheres to ellipsoids. The particle aspect ratio ranges between 1 (spheres) and 2.3, with a mean value of 1.4 and a standard deviation of 0.3. Most of the nanoparticles display quasi-spherical shape with diameter in the range of 40–180 nm (mean value of 80 nm). They have an onion-like structure and are composed of concentric WS_2 layers evenly spaced by 6.18 Å. Its hollow nature is reflected by the contrast difference in the core, and the dimension of the hollow void in the centre is about half the overall nanoparticle diameter. The iPP/IF-WS_2 nanocomposites (0.05–8.0 wt% nanoparticle loading) were prepared via melt-blending in a Haake Rheocord 90 extruder operating at 210 °C, with mixing times of 10 min and a rotor speed of 150 rpm. Subsequently, a small amount of the extruded material was used to fabricate films in a hot-press at 210 °C under successive pressures of 10, 50 and 120 bars during 2 min at each pressure.

2.2. Materials characterization

Tensile tests were carried out on a servo-hydraulic testing machine (type MTS 858) equipped with a controlled temperature chamber at 23, 35, 50, 65 and 80 °C. Dog-bone tensile coupons were employed, according to the ASTM D638 standard. Specimens were conditioned at the testing temperature and 50 ± 5% RH for 24 h prior to the measurements. The cross-head speeds applied were in the range of 1–100 mm min^{-1}, corresponding to relative strain rates between 6.67 × 10^{-4} and 6.67 × 10^{-2} s^{-1}. Five specimens at each cross-head speed and fixed temperature were tested for each sample, and the data reported correspond to the average value. The fractured surfaces of tensile coupons of iPP and the nanocomposites were observed using a Philips XL30 scanning electron microscope

(SEM) operating at 25 kV. Prior to examination, specimens were coated with a ~5 nm Au/Pd overlayer to avoid charging during electron irradiation.

The HDT was measured using an HDT/VICAT heat deflection tester according to ASTM D648 standard. Specimens were conditioned at 25 ± 2 °C and 50 ± 5% RH for 24 h prior to the measurements. The sample position was edgewise, test span 100 mm, the surface stress 1.8 MPa and the heating rate 2 °C min^{-1}.

The CTE of iPP based nanocomposites was measured across the thickness using a Perkin–Elmer TMA 7 thermomechanical analyzer. Samples of ~7 mm × 7 mm size were heated from −25 to 150 °C at rate of 2 °C min^{-1} under nitrogen atmosphere. T_g was identified as the temperature at which the slope of the TMA plot change, and the CTE was determined both below and above T_g.

The effective through-plane thermal conductivity (K) of the nanocomposites was determined using a KES-F7 Thermo Labo type II device equipped with a temperature controlled hot plate and placed in a thermostatic chamber to be kept in a constant operating environment. The effect of the contact thermal resistance was removed by measuring the thermal conductivity of a reference material. K was calculated using the equation $K = tW/(T_{hot} - T_{cold})A$, where t is the sample thickness, W is the heat flow, T_{hot} and T_{cold} are the temperatures of the hot and cold plates, respectively, and A is the surface area of the hot plate (2.5 × 2.5 mm^2). Five specimens for each sample were tested and the average value is reported.

Flammability properties including the ignition point and heat release rate (HRR) were measured with a cone calorimeter according to the ASTM E1356 standard. An external radiant heat flux of 50 kW m^{-2} was applied. All the samples were measured in the horizontal position and wrapped with thin aluminium foil except for the irradiated sample surface. Prior to the experiments, samples were conditioned at 23 ± 2 °C and 50 ± 5% RH for 1 week. The materials were tested in triplicate to ensure repeatability.

3. Results and discussion

3.1. Tensile behaviour

Fig. 1 shows typical stress–strain curves of neat iPP and iPP/IF-WS_2 nanocomposites incorporating different nanoparticle contents at 23 °C and a strain rate of 6.67 × 10^{-4} s^{-1}. All the samples present a linear elastic behaviour at the beginning of the tensile tests and a region of plastic deformation before the fracture. As can be observed, the incorporation of very small amounts (0.05–1.0 wt%)

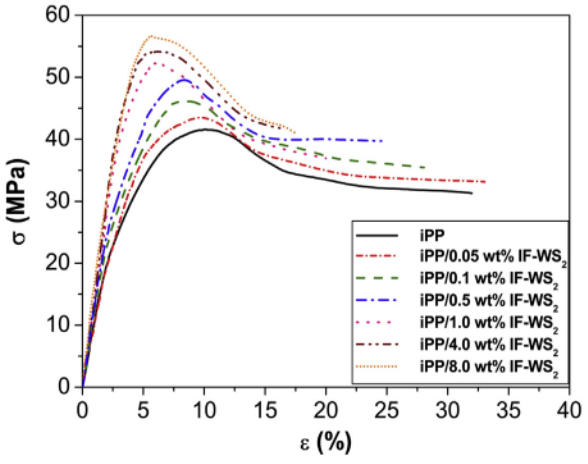

Fig. 1. Stress–strain curves of neat iPP and iPP/IF-WS_2 nanocomposites at 23 °C and a strain rate of 6.67 × 10^{-4} s^{-1}.

of IF-WS_2 into this thermoplastic results in a sharp improvement in its Young's modulus (E) and yield strength (σ_y), by up to 38 and 27%, respectively, at 1.0 wt% loading. Further raise in the nanofiller loading also leads to an enhancement in these tensile properties, albeit the increases are less accentuated (i.e. 46 and 36% over neat iPP at 8.0 wt% loading, respectively). Similar relative increments were obtained for the other strain rates tested. This behaviour can be more clearly visualized in Fig. 2a and b, which present the evolution of E and σ_y as a function of the IF-WS_2 content. A non-linear growth in the modulus and strength is detected, the increase being considerably more pronounced at very low concentrations. This trend should be related with the nucleating effect of these nanoparticles on the α-crystalline form, since changes in the level of crystallinity of the nanocomposites are known to have strong influence on the mechanical performance of the materials. Thus, according to DSC analysis [14], the nucleating efficiency (NE) of the IF-WS_2 was found to increase drastically up to 60% at 2.0 wt% loading while at higher contents it was approximately maintained. The strong stiffness and strength enhancements obtained at low nanoparticle loadings are mainly associated with the increase in crystallinity caused by heterogeneous nucleation, while the additional improvements attained at higher loadings are ascribed to conventional reinforcement effects. It is worthy to notice that, comparing the results obtained at room temperature and similar strain rates, the improvements attained in the nanocomposite filled with 1.0 wt% IF-WS_2 are higher than those obtained with the same amount of nano-SiO_2 [7,23] or CNTs (either SWCNTs [9] or multi-walled carbon nanotubes, MWCNTs [22]). Moreover, the maximum stiffness and strength enhancements achieved upon addition of the IF-WS_2 nanoparticles are also higher than those reached with the other nanofillers, which should arise from a better dispersion and adhesion with the matrix, factors that are extremely important for improving the mechanical behaviour of composites. Thus, CNTs are typically grouped in bundles due to their intrinsic van der Waals forces; in addition, their large aspect ratio causes very high viscosity in the polymer melt that hinders their uniform dispersion without the aid of surfactants or compatibilizing agents at loadings ≥1.0 wt% [24]. Analogously, the presence of hydroxyl groups on the surface of silica nanoparticles increases their tendency to form aggregates via hydrogen bond creation, and the size of the agglomerates enlarges considerably for concentrations >3.0 wt% [23]. In contrast, the lubricant character of the IF-WS_2 makes possible to attain a very uniform dispersion within the matrix, as can be clearly observed from Fig. 3 that presents SEM images of fractured surfaces of composites with different nanofiller loadings. For IF-WS_2 contents up to 4.0 wt%, the individual nanoparticles are randomly distributed inside the polymer and exhibit a near spherical shape with an average diameter of 90 nm, in agreement with the size of the as-received particles [14]. A homogeneous IF-WS_2 distribution is also observed at 8.0 wt% loading, albeit small clusters of 2–4 particles can be found. The high IF-WS_2 specific surface area enables the formation of a large interphase in the nanocomposite and strong iPP-nanoparticle interactions, hence facilitating the stress transfer, which combined with their high modulus and low cost make them ideal fillers to reinforce polymeric matrices.

The Young's modulus of polymer nanocomposites can be predicted by the Krenchel's rule of mixtures for discontinuous reinforcement [25]:

$$E_c = \left(\eta E_f - E_m\right)V_f + E_m \quad (1)$$

where E_f and E_m are the modulus of the filler and matrix, respectively, V_f the filler volume fraction and η the strengthening

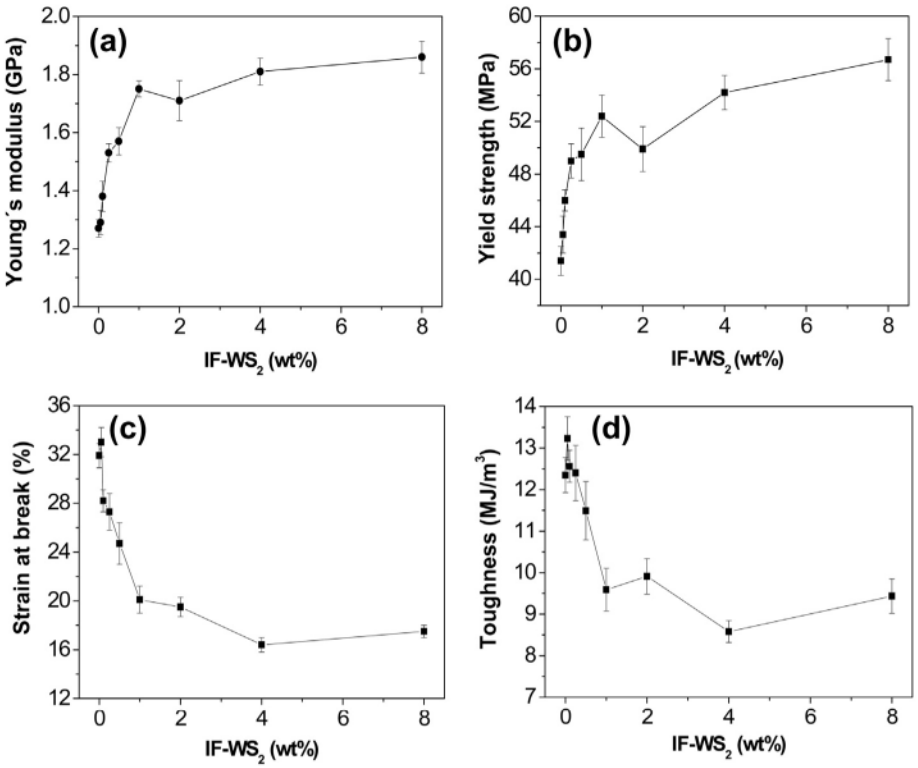

Fig. 2. Young's modulus, yield strength, strain at break and toughness of iPP/IF-WS_2 nanocomposites at 23 °C and a strain rate of 6.67×10^{-4} s^{-1} as a function of the nanoparticle loading.

efficiency coefficient that is assumed to be 1/5 for randomly oriented fillers. Considering the reported modulus for the IF-WS_2 (~160 GPa) [12], the theoretical values for the nanocomposites with different nanoparticle contents were evaluated using Eq. (1), and the results are tabulated in Table 1. The experimental values systematically exceed the theoretical calculations (up to 25%), and in general the differences grow with increasing IF-WS_2 concentration albeit the modulus of the composite with 8.0 wt% loading is in good agreement with the predictions. As mentioned above, for nanoparticle contents up to 4.0 wt%, a very homogenous dispersion is attained, hence very effective reinforcement effect. In the case of the nanocomposite with 8.0 wt% IF-WS_2, the presence of small nanoparticle clusters likely results in a less efficient reinforcement, hence reducing the difference between the experimental and calculated data. On the other hand, the increase in modulus attained in the iPP/IF-WS_2 nanocomposites partly arises from the extra crystallinity, not solely from direct reinforcement. The model assumes that the modulus of each phase is independent and remains unchanged by the presence of the others components, while the IF-WS_2 act as nucleating agents that promote the crystallization of iPP near their surfaces [14], thus altering the polymer. Consequently, the properties of the interfacial matrix likely differ from those of neat iPP, and this probably contributes to the deviation from the theoretical predictions.

With regard to the strain at break (ε_b), Fig. 2c, the behaviour observed is opposite to that found for E and σ_y, showing a sharp drop (~35%) up to 1.0 wt% nanoparticle loading and then decreasing smoothly. This indicates that small amounts of IF-WS_2 restrict considerably the ductile flow of the matrix. This trend is in contrast to that reported for iPP/SiO_2 [7] or iPP/MWCNT [22] nanocomposites, where the addition of nanofillers hardly modified the plastic deformation of the polymer. The discrepancy could be ascribed to the more uniform dispersion of the IF nanoparticles, thus they act more effectively as a barrier for the mobility of the polymer chains. On the other hand, the area under the tensile curve is the strain energy per unit volume absorbed by the material, and is a measure of the impact resistance of the nanocomposites. This area is sensitive to the nanoparticle concentration (Fig. 2d): it remains merely unaffected in the range of 0–0.5 wt% and then falls progressively with increasing IF-WS_2 loading up to 4.0 wt% where the decrease in comparison to that of neat iPP is about 30%. This behaviour should be related to the α-nucleating effect of these nanoparticles [14], since the α-phase of iPP shows excellent modulus and tensile strength albeit poor fracture toughness. The results reveal that the addition of low IF-WS_2 loadings provides a good balance between stiffness and impact strength, while at concentrations ≥1.0 wt% the increase in modulus is attained at the expense of ductility and toughness.

The mechanical properties of polymer nanocomposites depend strongly on the deformation rate; the effect of this parameter is one of the best indicators to evaluate the performance of a material under dynamic loading. Fig. 4 shows typical stress–strain curves of iPP/IF-WS_2 (1.0 wt%) nanocomposite at 23 °C and different strain rates. The curves exhibit three distinct zones: an initial linear elasticity, a non-linear transition to the maximum stress or yield point (σ_y) and a stress drop or softening. At the yield stress, a small neck is formed within the gauge length of the specimen and the molecules tend to align along the direction of the applied load, hence the material becomes stiffer. Analogous cold-drawing behaviour was observed for neat iPP and the other nanocomposites tested. Nevertheless, the yielding behaviour is found to be strain rate sensitive: with increasing rate, the Young's modulus and yield strength significantly rise, the yield strain drops and the sample fails with little cold-drawing in a more brittle failure mode. This could be attributed to a decrease in the molecular mobility of the polymer chains, hence making the nanocomposite stiffer and

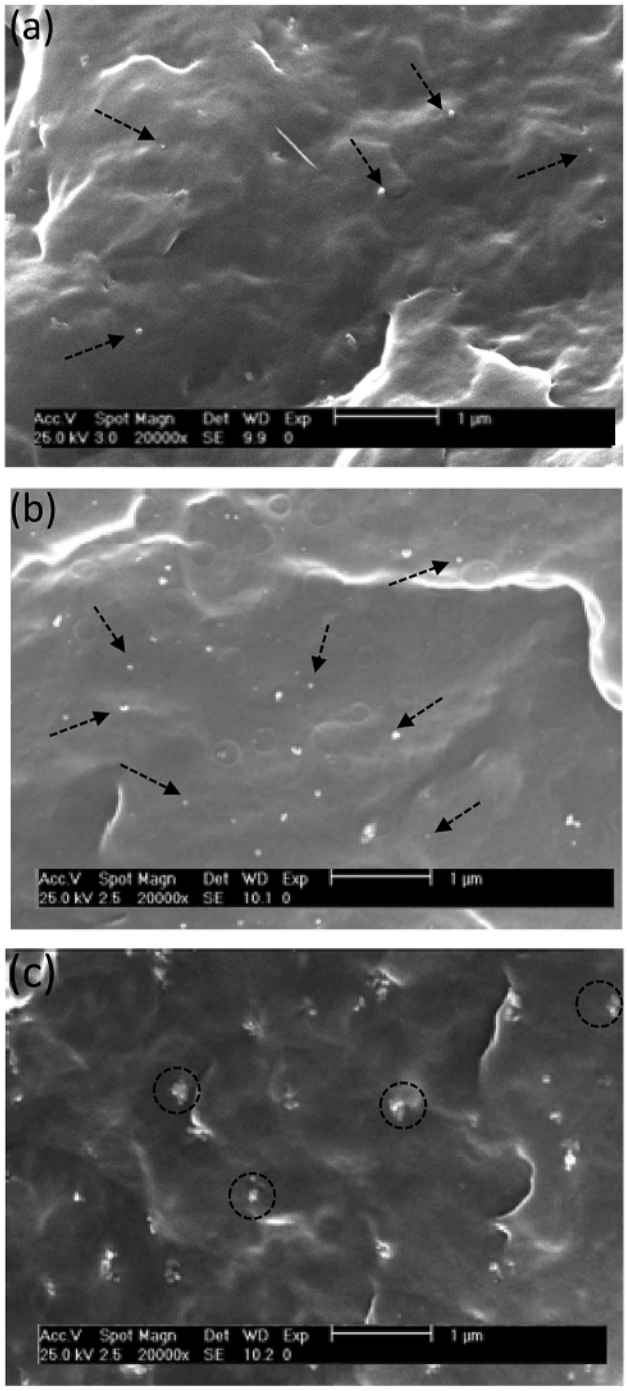

Fig. 3. SEM micrographs from fractured surfaces of iPP/IF-WS_2 nanocomposites with nanofiller loadings of (a) 2.0, (b) 4.0 and (c) 8.0 wt%. The dashed arrows point individual nanoparticles randomly dispersed within the matrix. The circles in (c) show small clusters of 2–4 particles.

stronger [23]. Further, this yield stress enhancement could also be ascribed to a shift in the molecular relaxations of polymeric materials during impact, as reported previously [26], since the heat accumulated upon application of high strain rates can slightly alter the glass transition. Thus, at low deformation rates the polymer matrix is in a rubbery-like regime, whereas at high rates it changes to a leathery regime where the intermolecular interactions between chains in the amorphous region impose strong resistance tow7ards deformation. Consequently, the higher the strain rate applied to the nanocomposites, the higher the modulus and yield stress.

The σ_y values for iPP and iPP/IF-WS_2 nanocomposites obtained at 23 °C and different strain rates are tabulated in Table 2. For all the samples tested, σ_y increases progressively with increasing loading rate, and for each rate it rises with the nanoparticle content following similar trend to that depicted in Fig. 2b. The yield strength of polymeric materials is sensitive to the strain rate and temperature, and can be described by the Eyring's equation [27] in which the yielding is considered an energy-activated rate dependent phenomenon:

$$\sigma_y = \frac{\Delta U}{v} + \frac{RT}{v} \times \ln \frac{2\dot{\varepsilon}}{e_0} \tag{2}$$

where T is the test temperature in Kelvin, ΔU is the activation energy for plastic deformation (i.e. the height of the potential energy barrier of two adjacent equilibrium positions for element units to jump), v is the activation volume of the element motion unit, $\dot{\varepsilon}$ is the strain rate, e_0 the pre-exponential factor and R the gas constant. The activation volume is an important parameter that provides information about the deformation mechanism of the material. The plot of σ_y vs. ln $(\dot{\varepsilon})$ at different temperatures provides parallel straight lines with the same slope given by RT/v. The activation volume can subsequently be determined from this slope. The intercept of this plot at $\dot{\varepsilon} = 1$ is equal to $(\Delta U/v) - (RT \ln e_0/v)$. Since RT/v is constant, a plot of $(\Delta U/v) - (RT \ln e_0/v)$ vs. $1/v$, if linear, yields the value of ΔU. The inset of Fig. 4 shows, as an example, σ_y vs. ln $(\dot{\varepsilon})$ data for iPP/IF-WS_2 (1.0 wt%) nanocomposite over the strain rate range investigated at 23 °C. Similar plots were obtained for the other nanocomposites, and the slopes of the regression lines are collected in Table 2. Clearly, the value of the slope rises with increasing IF-WS_2 concentration, the increase being more pronounced at low loadings. The activation volumes calculated at different temperatures and the activation energies are listed in Table 3. The experimental v for neat iPP is in good agreement to that previously reported by other researches [28], who suggested that the plastic flow is controlled by the cooperative motion of the polymer chains. For a given temperature, the addition of IF-WS_2 leads to a progressive drop in v up to 1.0 wt% loading, where the decrease is on average 22%, while further increase in the nanoparticle content hardly modifies the activation volume. This confirms that low amounts of IF-WS_2 strongly hinder the mobility of the matrix chain segments, due to their very homogenous dispersion and large interfacial contact area with the matrix chains. Qualitatively analogous reduction in v has been described for iPP/MWCNT nanocomposites [22], whereas an opposite behaviour has been reported for iPP/talc composites [3], where the microfillers did not produce a strengthening effect. As expected, the activation volume of all the samples rises with increasing temperature, by around 20% over the range 23–80 °C, pointing out that all of them display similar temperature sensitivity. However, the activation energy is independent of this parameter, albeit increases slightly as the IF-WS_2 concentration rises (up to ~9% increment at the highest loading tested), which further corroborates that these nanoparticles effectively restrict chain motion, thereby leading to a very efficient reinforcement effect. To obtain more information about the influence of the strain rate on the failure mode of these nanocomposites, the fractured surfaces of tensile specimens were examined by SEM, and typical images of iPP/IF-WS_2 (1.0 wt%) nanocomposite after stretching at 23 °C are shown in Fig. 5. As can be observed, at a high strain rate of 6.67×10^{-2} s^{-1} (Fig. 5a) the sample surface appears to be quite flat and smooth, characteristic of a relatively brittle fracture, and several small cracks nucleating at the same time from different regions are detected, which serve as stress concentration

Table 1
Experimental and calculated Young's modulus E and thermal conductivity K values at room temperature for iPP/IF-WS_2 nanocomposites.

IF-WS_2 content (wt%)	E_{exp} (GPa)	E_{cal}[a] (GPa)	$(E_{cal} - E_{exp})/E_{exp}$ (%)	K_{exp}[b] (W m^{-1} K^{-1})	K_{cal} (W m^{-1} K^{-1})	$(K_{cal} - K_{exp})/K_{exp}$ (%)
0.0	1.27 ± 0.03	–	–	0.22 ± 0.01	–	–
0.05	1.29 ± 0.04	1.27	−1.4	0.21 ± 0.01	0.22	+4.7
0.1	1.39 ± 0.05	1.27	−8.6	0.24 ± 0.02	0.22	−7.3
0.25	1.53 ± 0.03	1.28	−16.1	0.24 ± 0.01	0.22	−8.6
0.5	1.57 ± 0.05	1.30	−17.5	0.25 ± 0.02	0.22	−11.2
1.0	1.75 ± 0.03	1.31	−25.0	0.27 ± 0.01	0.22	−17.4
2.0	1.71 ± 0.07	1.35	−20.8	0.27 ± 0.01	0.22	−18.0
4.0	1.81 ± 0.05	1.43	−20.9	0.29 ± 0.02	0.23	−21.4
8.0	1.85 ± 0.06	1.72	−6.9	0.30 ± 0.02	0.24	−21.7

[a] Values calculated through the Krenchel's rule of mixtures.
[b] Values estimated using the Maxwell model.

sites in the matrix and eventually coalesce, leading to premature failure. However, the nanoparticles are homogenously dispersed within the matrix and act effectively as a barrier for pining and bifurcation of the advancing cracks. In contrast, at a low strain rate of 6.67 × 10^{-4} s^{-1} (Fig. 5b) the nanocomposite exhibits a rough fractured surface without evident cracks, and some spherical dimples are observed typical of a ductile failure. In this case, the movement of the polymer chains can follow the deformation induced by the applied load, resulting in a higher degree of plastic deformation. These SEM observations are consistent with the results derived from the tensile tests, which revealed that the nanocomposites showed necking and cold-drawing behaviour at low strain rates while failed in a brittle mode at higher rates.

The influence of temperature on the tensile behaviour of iPP/IF-WS_2 nanocomposites was also investigated, and the experimental data demonstrated that these nanomaterials are extremely temperature sensitive. Fig. 6 shows, as an example, typical stress–strain curves for neat iPP (a) and the nanocomposite with 1.0 wt% nanoparticle loading (b) at different temperatures above T_g (see the following section) and a strain rate of 6.67 × 10^{-4} s^{-1}. An analogous behaviour was found for the rest of the nanocomposites tested. As expected, the Young's modulus and yield strength drop as the temperature rises due to the increased plasticization of the polymer, while the strain at break and area under the tensile curve increase. As can be more clearly visualized in the inset of Fig. 6b, E drops sharply (~45%) in the range of 23–50 °C, temperature interval close to T_g, and then falls moderately (~25%) up to 80 °C,

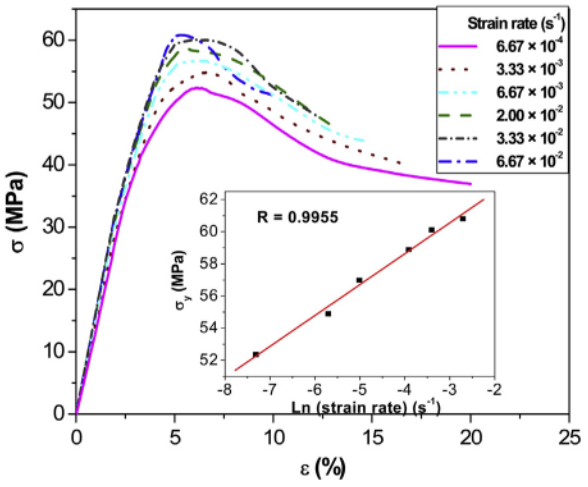

Fig. 4. Stress–strain curves of iPP/IF-WS_2 (1.0 wt%) nanocomposite at 23 °C and different strain rates. The inset shows the plot of the yield strength σ_y vs. ln (strain rate) and the straight line represents the linear fit to the Eyring's equation.

while ε_b displays an opposite trend. Fig. 7a presents σ_y values vs. temperature (T) for neat iPP and the different nanocomposites at the mentioned strain rate. A non-linear decay is detected for all the samples, the descent being more marked at low temperatures, similarly to the behaviour found for the modulus. To evaluate the change in the reinforcing efficiency of these nanoparticles with temperature, the relative increment in yield strength ($\Delta\sigma_y$) in comparison to neat iPP was plotted as a function of T for the different nanocomposites, and the curves are depicted in Fig. 7b. In general, the reinforcing efficiency is greater at higher temperatures (i.e. 60% increase in $\Delta\sigma_y$ from 23 to 80 °C at 2.0 wt% IF-WS_2 loading), which can be explained considering that the nanoparticles hinder the plastic deformation of the iPP matrix which is accentuated at high temperatures. Qualitatively analogous behaviour has been reported for different thermoplastic based nanocomposites such as iPP/MWCNT [22] or nylon 6/halloysite [29]. Nonetheless, this trend becomes slightly less pronounced with increasing nanoparticle content, and for the nanocomposite with 8.0 wt% loading $\Delta\sigma_y$ remains merely unchanged over the temperature range studied. Further, the reinforcing efficiency increases sharply at very low nanoparticle concentrations until it reaches 1.0 wt% and then grows only slightly, being this effect even more pronounced at high temperatures. Therefore, 1.0 wt% appears to be a critical concentration that probably corresponds to the formation of a well-dispersed nanoparticle network all over the nanocomposite that acts as an effective barrier for the mobility of the chain segments in the amorphous region. Further increase in the nanoparticle content would hardly provide additional constraints on polymer chain motion, hence $\Delta\sigma_y$ remains approximately constant. Overall, the results confirm that matrix-dominated mechanical properties such as tensile are enhanced by adding IF-WS_2 nanoparticles, and the extent of the improvement depends strongly on the nanofiller loading as well as on environmental factors such as temperature and strain rate.

3.2. Thermomechanical properties

Table 4 summarizes T_g values for the iPP/IF-WS_2 nanocomposites obtained from TMA measurements. T_g is indicative of the motion of the polymer chains in the amorphous region. In the neat matrix, the chain segments are free from restraints. The presence of the IF-WS_2 decreases the free volume of the polymeric network, which combined with their very homogenous dispersion and large iPP-nanoparticle interfacial contact area provokes an effective immobilization of the matrix chains, thereby raising T_g. Thus, the value for neat iPP is around 4 °C, and increases by up to 5 °C at 1.0 wt% loading. However, further rise in the IF-WS_2 concentration hardly modifies T_g, which is consistent with the trend described previously for the Young's modulus and yield strength.

Table 2
Yield strength σ_y for iPP and iPP/IF-WS_2 nanocomposites at 23 °C for various strain rates ($\dot{\varepsilon}$) and slope of the plot σ_y vs. ln ($\dot{\varepsilon}$).

IF-WS_2 content (wt%)	Strain rate $\dot{\varepsilon}$ (s^{-1})						Slope (MPa)
	6.67×10^{-4}	3.33×10^{-3}	6.67×10^{-3}	2.00×10^{-2}	3.33×10^{-2}	6.67×10^{-2}	RT/v
0.0	41.4 ± 1.1	44.2 ± 1.5	45.1 ± 0.9	46.7 ± 1.0	47.5 ± 1.3	48.1 ± 1.2	1.47 ± 0.05
0.05	43.4 ± 1.4	46.4 ± 0.9	47.3 ± 1.3	49.1 ± 0.8	49.8 ± 1.5	50.6 ± 1.3	1.56 ± 0.05
0.1	46.0 ± 0.8	49.2 ± 1.3	50.2 ± 1.6	52.0 ± 1.2	52.8 ± 1.7	53.6 ± 1.9	1.65 ± 0.06
0.25	49.0 ± 1.3	52.2 ± 1.3	53.2 ± 2.3	55.1 ± 1.1	56.0 ± 2.0	56.9 ± 2.2	1.71 ± 0.05
0.5	49.5 ± 2.0	52.6 ± 1.6	53.7 ± 1.8	55.6 ± 2.1	56.5 ± 1.4	57.3 ± 1.4	1.70 ± 0.04
1.0	52.4 ± 1.6	54.9 ± 1.3	57.0 ± 1.4	58.7 ± 1.8	60.1 ± 0.9	60.7 ± 1.1	1.88 ± 0.08
2.0	49.9 ± 1.7	52.1 ± 1.5	54.1 ± 1.3	55.7 ± 1.6	57.0 ± 1.9	57.7 ± 2.0	1.75 ± 0.08
4.0	54.2 ± 1.3	57.8 ± 0.9	59.6 ± 1.6	61.1 ± 1.4	62.0 ± 1.2	63.0 ± 1.7	1.89 ± 0.09
8.0	56.3 ± 1.6	59.8 ± 2.1	61.1 ± 1.9	62.9 ± 2.3	64.1 ± 1.7	65.0 ± 1.5	1.91 ± 0.07

An analogous behaviour of T_g increase has been previously reported for different iPP based nanocomposites using DMA technique [9,22,30]. Interestingly, for the same nanofiller concentration, the temperature shift attained with the IF nanoparticles is larger than that obtained upon addition of nanosilica [30] or MWCNTs [22], and is comparable to that found for iPP/SWCNT composites [9].

The CTE is a key thermomechanical property used in the design of composites for structural applications. A low CTE is desirable to maintain the dimensional stability of the material. In polymer nanocomposites, a low CTE can be attained by dispersing hard nanofillers with low CTE inside the matrix. Inorganic nanoparticles are known to have low CTE [31], hence it is expected that the addition of IF-WS_2 has a significant effect on this property. Table 4 collects the CTE data at −20 and 25 °C measured across the thickness of the specimens using TMA technique. At $T < T_g$, the CTE of neat iPP is around 62×10^{-6} °C^{-1}, and decreases steadily with increasing IF-WS_2 loadings, by up to 22% for iPP/IF-WS_2 (8.0 wt%). Such remarkable reduction is attributed to the increase in the stiffness and strength of the matrix due to the presence of these nanoparticles. Additionally, this noticeable reduction should be related to the intrinsic characteristics of the IF-WS_2 (i.e. layered structure, small diameter, quasi-spherical shape and low CTE).

On the other hand, the CTE values at $T > T_g$ are considerably higher than those measured in the glassy state, though the dependence on the IF-WS_2 concentration is qualitatively similar for both testing temperatures. Nevertheless, the drop in CTE for a given nanoparticle loading is more marked in the rubbery state (i.e. about 31% for the nanocomposite with the highest IF-WS_2 loading compared to that of neat iPP). The stronger CTE reduction above T_g probably arises from the larger differences in stiffness and thermal expansion coefficients between iPP and the nanoparticles, as previously reported for other thermoplastic/organoclay nanocomposites [32]. Moreover, the IF-WS_2 possess large specific surface area, hence can greatly absorb the heat transferred from the matrix, and in turn significantly suppress the thermal expansion of the plastic polymer in the rubbery state. Using also TMA measurements, Kalaitzidou et al. [33] compared the CTE of PP composites reinforced with different carbon fillers. In the glassy state, a reduction of around 25% was attained upon incorporation of ~7 wt% graphite nanoplatelets or carbon fibres, comparable to that obtained with 8.0 wt% IF-WS_2. In the rubbery state, the carbon fillers led to a diminution of ~20%, smaller than that obtained with the IF-WS_2.

The HDT is an indicator of the heat resistance of a material under a specified load, and is an important parameter when a material is being used for high-temperature structural applications. The incorporation of hard nanofillers such as clays [34] or CNTs [22] into thermoplastic matrices has been reported to improve the HDT. The data for the iPP/IF-WS_2 nanocomposites are tabulated in Table 4. As can be observed, the HDT continuously grows with increasing IF-WS_2 concentration, from 66 °C for neat iPP up to 85 °C (~29% increase) at 8.0 wt% loading. This significant enhancement should arise from the rise in stiffness and strength as well as from the good dispersion of the nanoparticles that provide effective reinforcement to the iPP matrix. As known, the HDT of a polymer can be enhanced by increasing T_g, raising the crystallinity and/or reinforcing. In iPP/IF-WS_2 nanocomposites, these three factors rise upon increasing nanofiller concentration, particularly at very low loadings, thereby resulting in a synergistic effect on enhancing the matrix HDT. Thus, the increment attained at 1.0 wt% IF-WS_2 loading (~24%) is larger than that obtained from DMA measurements upon incorporation of the same amount of MWCNTs to neat iPP [22]. The aforementioned results underline the potential of using IF-nanoparticles for enhancing the thermomechanical properties of thermoplastic polymers.

3.3. Thermal conductivity and flammability

The incorporation of thermally conductive fillers such as graphite, CNTs, carbon fibres, ceramic or metallic particles into polymers can enhance the thermal conductivity (K) for applications such as lighting ballasts, transformer housings, microchip cooling, fuses, radiators, etc. [33]. The most important factors that influence K of polymeric nanocomposites are the filler thermal conductivity,

Table 3
Activation volumes v at different temperatures calculated according to the Eyring's equation and activation energy ΔU for iPP and iPP/IF-WS_2 nanocomposites.

IF-WS_2 content (wt%)	$v_{23°C}$ (nm^3)	$v_{35°C}$ (nm^3)	$v_{50°C}$ (nm^3)	$v_{65°C}$ (nm^3)	$v_{80°C}$ (nm^3)	ΔU (KJ mol^{-1})
0.0	2.77 ± 0.09	2.89 ± 0.07	3.03 ± 0.09	3.17 ± 0.10	3.31 ± 0.11	221 ± 8
0.05	2.62 ± 0.08	2.72 ± 0.06	2.85 ± 0.10	2.98 ± 0.09	3.12 ± 0.12	216 ± 12
0.1	2.47 ± 0.09	2.57 ± 0.08	2.69 ± 0.12	2.82 ± 0.13	2.95 ± 0.09	226 ± 11
0.25	2.39 ± 0.07	2.48 ± 0.13	2.60 ± 0.11	2.72 ± 0.15	2.85 ± 0.08	229 ± 9
0.5	2.40 ± 0.06	2.49 ± 0.12	2.62 ± 0.14	2.73 ± 0.08	2.86 ± 0.11	227 ± 10
1.0	2.17 ± 0.09	2.26 ± 0.06	2.37 ± 0.09	2.48 ± 0.08	2.59 ± 0.11	234 ± 10
2.0	2.33 ± 0.10	2.43 ± 0.14	2.55 ± 0.13	2.66 ± 0.11	2.78 ± 0.15	230 ± 9
4.0	2.16 ± 0.10	2.25 ± 0.13	2.36 ± 0.12	2.47 ± 0.09	2.57 ± 0.06	235 ± 11
8.0	2.14 ± 0.08	2.23 ± 0.12	2.34 ± 0.14	2.44 ± 0.08	2.55 ± 0.09	239 ± 12

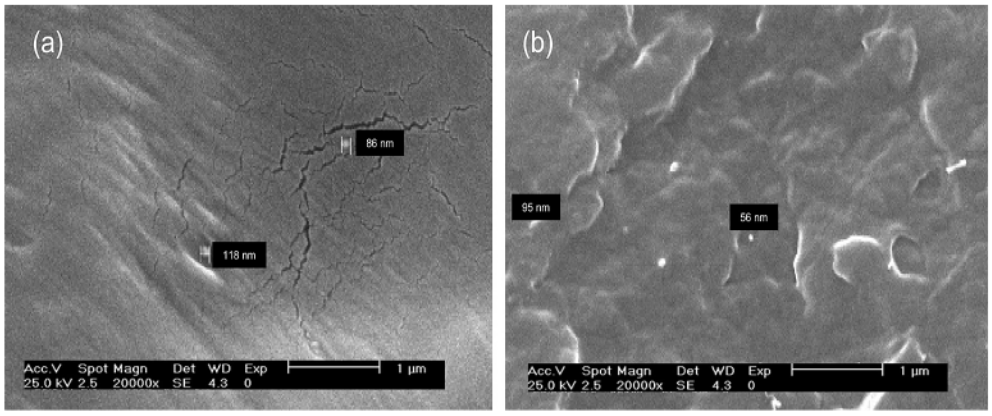

Fig. 5. SEM images of the fractured surface of iPP/IF-WS_2 (1.0 wt%) nanocomposite after stretching at 23 °C and a strain rate of (a) 6.67 × 10^{-2} s^{-1} and (b) 6.67 × 10^{-4} s^{-1}.

purity, size, aspect ratio, concentration and state of dispersion as well as the nature, molecular weight, structural defects and degree of crystallinity of the polymer. The temperature dependence of K for neat iPP and the IF-WS_2 reinforced nanocomposites is compared in Fig. 8a. In the low temperature range ($T < T_g$), K of neat iPP increases almost linearly with temperature; in the interval between 0 and 120 °C it remains approximately constant and then falls slightly at higher T. This behaviour is consistent to that previously reported by other authors [35]. Regarding the nanocomposites, the trend observed is qualitatively similar to that described for the pure polymer: K rises steadily in the glassy state, ascribed to a gradual increase in the phonon population [36], while becomes merely independent of temperature in the rubbery state, showing a slight drop in the vicinity of the melting point of the matrix likely to be caused by a modification of the phonon modes and the corresponding change in thermal transport. Interestingly, the average slope in the glassy state (dK/dT) grows gradually upon increasing nanoparticle concentration, from 4.05 × 10^{-4} W m^{-1} K^{-2} for iPP to

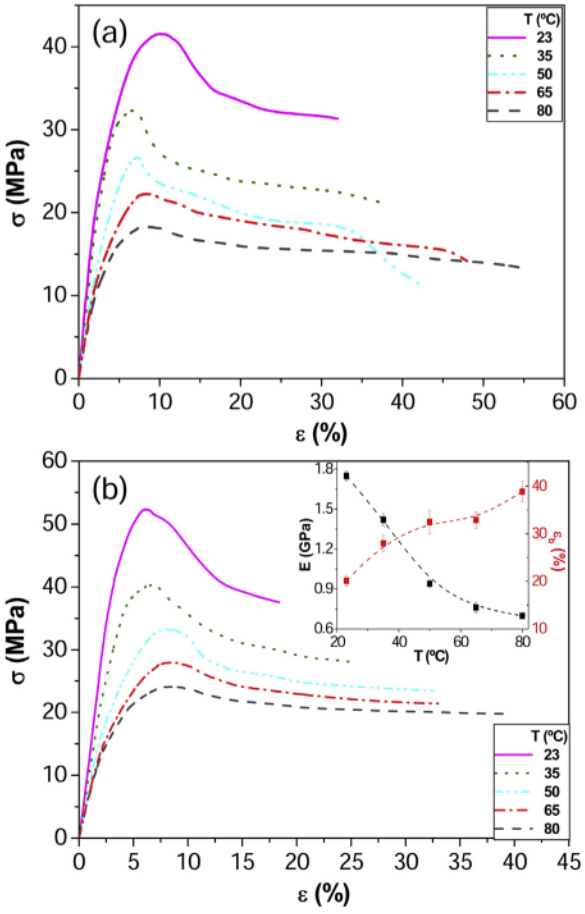

Fig. 6. Stress–strain curves of (a) neat iPP and (b) iPP/IF-WS_2 (1.0 wt%) nanocomposite at a strain rate of 6.67 × 10^{-4} s^{-1} and different temperatures. The inset in (b) shows the evolution of the Young's modulus E and strain at break ε_b as a function of temperature.

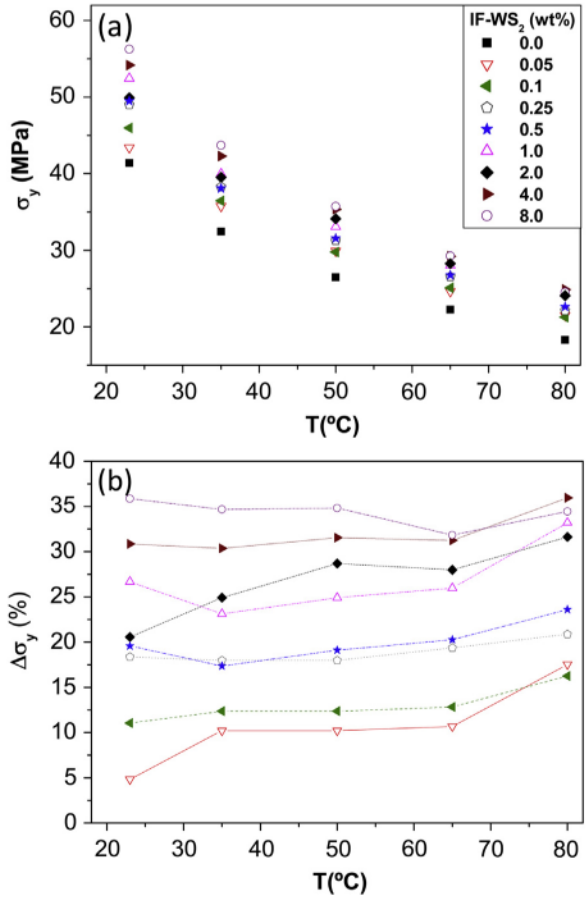

Fig. 7. (a): Yield strength σ_y vs. temperature for iPP and iPP/IF-WS_2 nanocomposites at a strain rate of 6.67 × 10^{-4} s^{-1}. (b): Percentage of increment in the yield strength vs. temperature.

Table 4
Thermomechanical properties for iPP and iPP/IF-WS_2 nanocomposites: Heat deflection temperature (HDT), glass transition temperature (T_g) and coefficient of thermal expansion (CTE).

IF-WS_2 content (wt%)	HDT (°C)	T_g (°C)	10^{-6} $CTE_{-20°C}$ ($°C^{-1}$)	10^{-6} $CTE_{25°C}$ ($°C^{-1}$)
0.0	65.8 ± 2.5	4.6 ± 0.3	62.4 ± 3.1	118.4 ± 5.6
0.05	67.2 ± 3.1	4.2 ± 0.5	60.8 ± 4.5	106.5 ± 6.8
0.1	73.4 ± 2.9	5.3 ± 1.1	58.3 ± 2.6	98.3 ± 4.6
0.25	77.6 ± 2.8	6.8 ± 0.6	55.9 ± 3.2	93.8 ± 5.3
0.5	75.3 ± 3.3	6.6 ± 0.7	55.4 ± 3.7	90.6 ± 5.0
1.0	81.9 ± 2.7	9.5 ± 0.8	52.6 ± 2.9	87.7 ± 4.2
2.0	80.6 ± 3.4	7.4 ± 0.4	52.5 ± 2.3	88.9 ± 4.1
4.0	83.4 ± 3.6	9.1 ± 0.5	50.2 ± 2.6	85.6 ± 3.6
8.0	85.1 ± 4.0	9.7 ± 0.9	48.7 ± 2.0	82.1 ± 3.0

6.55×10^{-4} W m^{-1} K^{-2} for the nanocomposite with 8.0 wt% IF-WS_2. This behaviour is probably related to the differences in the degree of crystallinity of the nanocomposites. At temperatures below T_g, K is influenced by the variation of the phonon mean free path due to structure scattering (i.e. phonon scattering at the interface between the amorphous and crystalline phases) and chain defect scattering [36]. With increasing nanoparticle concentration, the level of crystallinity rises, leading to the formation of a more ordered structure [14], hence reducing the phonon scattering at the nanoparticle–matrix interface, which in turn would result in higher thermal conductivity. Further, as the temperature rises, the vibrations of the polymeric chains surrounded by the IF-WS_2 increase, thereby enhancing the phonon propagation length. Thus, it is reasonable that composites with higher nanoparticle loading exhibit larger dK/dT.

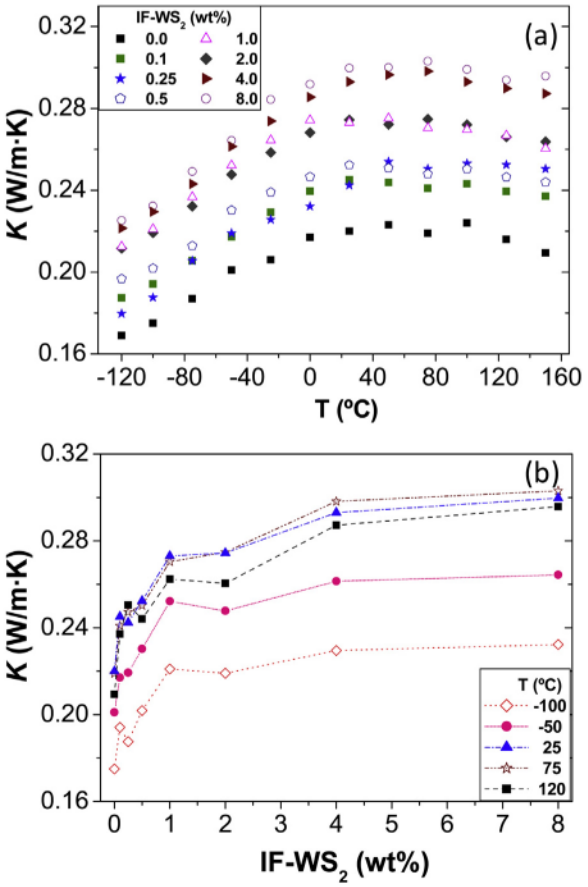

Fig. 8. (a): Comparison of the thermal conductivity (K) as a function of temperature for iPP/IF-WS_2 nanocomposites. (b): K vs. IF-WS_2 nanoparticle loading at different temperatures.

Fig. 8b presents the evolution of K as a function of IF-WS_2 loading for various selected temperatures. A clear increase in conductivity is observed upon addition of these nanoparticles both above and below T_g, which should arise from their higher K [37] compared to that of iPP combined with a very uniform dispersion and a strong interfacial adhesion with the polymer that promotes the conduction of phonons at the interface and minimizes the matrix coupling losses. Further, the nanoparticles act as α-nucleating agents, facilitating the crystallization of the polymer chains, and K of semicrystalline thermoplastics such as PP has been found to rise with crystallinity [36]. As can be observed, the increment in conductivity is considerably more pronounced at very low IF-WS_2 loadings, probably related with the NE of these nanoparticles that reaches a saturation level of ~60% at around 2 wt% [14]. It should also be noted that the extent of improvement is slightly more pronounced at $T > T_g$; thus, the maximum K increment attained at −100 °C is ~35%, while that at 120 °C is about 41%. A similar effect has been reported for PP/MWCNT nanocomposites [38], where K (measured using the line-source method) increased progressively with increasing nanotube loading up to 15 wt%, and the enhancement was particularly large above 160 °C. The room temperature K data for the different nanocomposites are listed in Table 1. The improvement in K of iPP attained upon addition of 8.0 wt% IF-WS_2 is ~37%, about half that determined from DSC measurements for composites incorporating ~7 wt% graphite nanoplatelets [33]. Nevertheless, taking into account that K of graphite is about five times larger than that of IF-WS_2 [37], one would expect that the thermal conductivities of iPP/graphite nanocomposites were considerably higher than those of iPP/IF-WS_2. The smaller differences found are ascribed to the poor dispersion of the nanoplatelets within the matrix, forming large agglomerates [33], which strongly limit the heat transfer. Further, the increase in K upon incorporation of 4.0 wt% IF-WS_2 (~32%) is comparable to that reported for PP/MWCNT (5.0 wt%) nanocomposite [38]; taking into account that CNTs exhibit a very high intrinsic thermal conductivity of 200–1000 W m^{-1} K^{-1}, their incorporation into iPP should have led to a drastic K increment. The small thermal conductance of the nanotube-polymer interface and the high interfacial thermal resistance between CNTs roped in bundles should account for the smaller enhancement.

The thermal conductivity of randomly distributed and non-interacting spheres in a homogeneous medium can be predicted by the Maxwell model [39]. For low nanoparticle volume fractions, the effective conductivity can be expressed as:

$$\frac{K_c}{K_m} = \frac{K_f + 2K_m + 2V_f\left(K_f - K_m\right)}{K_f + 2K_m - V_f\left(K_f - K_m\right)} \tag{3}$$

where K_c, K_m and K_f are the thermal conductivities of the composite, matrix and filler, respectively. Using Eq. (3), the theoretical values for iPP/IF-WS_2 nanocomposites were calculated and the results are summarized in Table 1. The experimental data are systematically higher than the theoretical predictions (up to 22% difference), and the discrepancies rise with increasing IF-WS_2 concentration. This behaviour can be explained taking into account that this classical model provides only a lower bound for the thermal conductivity of the composite, considers diffusive heat transfer in both continuous matrix and dispersed phases, and assumes that K_c depends solely on the volume fraction of the particles and the thermal conductivities of the components. However, K_c depends on a number of other parameters such as particle size,

shape, distribution, as well as particle–particle and particle–matrix interactions. Eq. (3) predicts well the thermal conductivity of composites with low filler concentration when K_f/K_m is high and the particle size is relatively large (on the micro- or millimetre scale). New models should be developed that could describe more accurately K of this type of nanocomposites. Overall, the results confirm that the incorporation of IF-WS_2 is a cheap an effective way for improving the thermal conductivity of thermoplastic polymers such as iPP, resulting in better heat transport and enhanced thermal stability for the nanocomposites [14].

In order to assess the flammability behaviour of the nanocomposites, cone calorimeter measurements were conducted on unfilled iPP and the nanocomposites. Fig. 9a shows the heat release rate (HRR) curves vs. testing time and Fig. 9b presents the ignition time (T_i), onset temperature at which begins the release of heat, and the peak HRR values for the different samples. Neat iPP begins releasing heat prior to the nanocomposites, in agreement with its lower thermal stability as revealed by TGA experiments [14]. The incorporation of increasing nanoparticle contents leads to a significant delay in the ignition time. Thus, T_i of iPP/IF-WS_2 (8 wt%) is 116 s, around 73% longer than that of the neat matrix (67 s). The peak HRR also occurs at much longer time for the nanocomposites (i.e. 263 s for the sample with 8.0 wt% IF-WS_2 compared to 189 s for the neat polymer). In contrast, the peak HRR value drops progressively with increasing IF-WS_2 concentration, from 1312 kW m^{-2} for iPP to 1196, 1152, 1072 and 1048 kW m^{-2} (decrements of 9, 12, 18 and 20%) for 0.1, 1.0, 4.0 and 8.0 wt% loadings, respectively. Using also cone calorimeter experiments, Kashiwagi et al. [38] studied the flame retardant performance of CNT filled PP and reported a reduction in the peak HRR of ~72% upon addition of 4.0 wt% MWCNTs. This strong enhancement was ascribed to the formation of a nanotube network layer covering the entire sample surface during burning without any significant cracks. A protective layer was also observed for PP/clay nanocomposites [40], albeit it was brittle and required a minimum of 5.0 wt% particles to cover the whole nanocomposite surface. Taking into account that no compact IF-WS_2 layer was observed on the residual samples from the cone experiments, it seems that the previously proposed fire retardant mechanism involving the formation of a reinforced clay or CNT char layer to prevent further burning is not a suitable explanation for the improvements in HRR in the case of the iPP/IF-WS_2 nanocomposites. The enhancements should be related to the superior thermal conductivity of the nanocomposites compared to that of iPP, as discussed previously. The nanoparticles help to dissipate the heat quickly through the bulk of the composite, which means that it takes longer for the surface temperature of the sample to reach the ignition point and the peak HRR. Another plausible explanation for the observed enhancements could be that the IF-WS_2 act as an insulator and mass transport barrier that hinder the escape of volatile products generated during the decomposition process and also prevent oxygen from reaching the matrix.

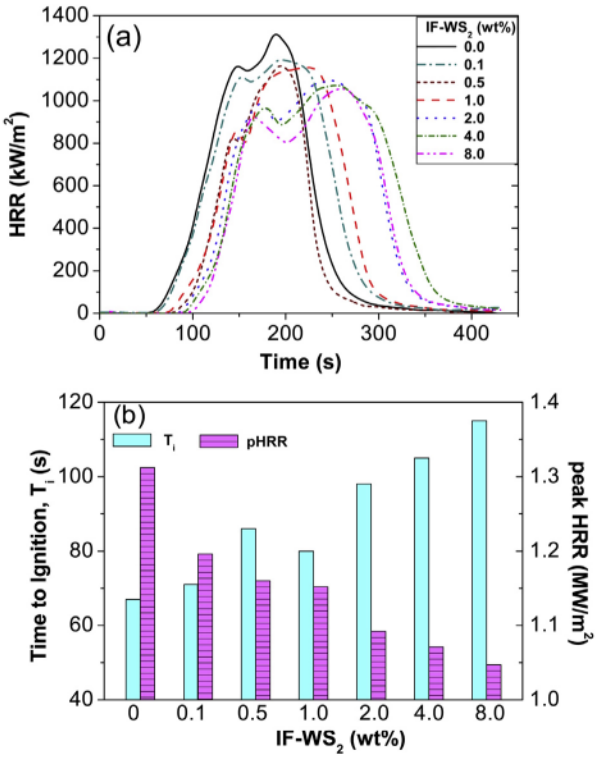

Fig. 9. (a): Heat release rate (HRR) vs. time curves obtained from cone tests experiments for iPP/IF-WS_2 nanocomposites. (b): Time to ignition T_i and peak HRR values for different nanoparticle loadings.

4. Conclusions

The influence of IF-WS_2 nanoparticles on the thermal and mechanical properties of iPP was studied. The addition of low IF-WS_2 contents remarkably enhanced the matrix Young's modulus and yield strength, particularly at high temperatures, and the increments attained were larger than those reported for similar amounts of other nanofillers like SiO_2 or CNTs. These strong improvements arise from a very homogenous IF-WS_2 dispersion, an effective load transfer induced by a large polymer-nanoparticle interfacial area combined with a rise in the level of crystallinity of iPP. Nevertheless, a drop in ductility and toughness was found at higher IF-WS_2 concentrations, since larger amounts of nanoparticles effectively restrict the ductile flow of the matrix chains. The nanocomposites were found to be extremely sensitive to strain rate and temperature, and their yield strength behaviour was accurately fitted by the energy-activated Eyring's equation. The activation energy increased while the activation volume decreased with increasing IF-WS_2 concentration, confirming a reduction in polymer chain mobility. The nanoparticles also improved the thermomechanical properties of iPP. A strong raise in the HDT and T_g while a significant drop in the CTE both in the glassy and rubbery states were detected. A noticeable increase in the thermal conductivity K was also found both above and below T_g. In the glassy state, K increased almost linearly with temperature, and the slope dK/dT grew steadily with the nanoparticle loading, due to a rise in crystallinity that reduces the phonon scattering at the nanoparticle–matrix interface. In the rubbery state, K became merely independent of temperature, showing a slight drop close to the melting point of the matrix likely to be caused by a modification of the phonon modes. The nanocomposites also exhibited superior flame retardancy: a progressive diminution in the peak HRR was found with increasing nanoparticle loading, combined with a delay in both the ignition point and the time of peak HRR. In general, the addition of IF-WS_2 is a cheaper and more effective way to improve the mechanical and thermal behaviour of thermoplastic polymers such as iPP compared to the incorporation of carbon nanofillers or other inorganic spherical nanoparticles. iPP/IF-WS_2 nanocomposites are highly suitable to be used in a wide range of industrial applications.

Acknowledgements

This work was supported by the Spanish Ministry of Science & Innovation in the Project MAT-2010-21070-C02-01. M.N. would like to acknowledge the Ministerio de Economía y Competitividad

(MINECO) for a 'Ramón y Cajal' senior research fellowship. A.D. would like to thank to the Consejo Superior de Investigaciones Científicas (CSIC) for a JAE postdoctoral contract.

References

[1] Y.S. Thio, A.S. Argon, R.E. Cohen, M. Weinberg, Polymer 43 (2002) 3661–3674.
[2] H. Shariatpanahi, F. Sarabi, M. Mirali, M. Hemmati, F. Mahdavi, J. Appl. Polym. Sci. 113 (2009) 922–926.
[3] L. Zhang, H. Liu, X. Qian, F. Liu, J. Zhang, J. Macromol. Sci. Part B 51 (2012) 1596–1605.
[4] M. Etcheverry, S.E. Barbosa, Materials 5 (2012) 1084–1113.
[5] S. Zhao, Z. Xin, J. Zhang, T. Han, J. Appl. Polym. Sci. 123 (2012) 617–626.
[6] D. Eirasa, L.A. Pessan, Mater. Res. 12 (2009) 517–522.
[7] A. Vassiliou, D. Vikiaris, E. Pavlidou, Macromol. React. Eng. 1 (2007) 488–501.
[8] M. Naffakh, V. López, F. Zamora, M.A. Gómez, Soft Mater. 8 (2010) 407–425.
[9] M.A.L. Manchado, L. Valentini, J. Biagiotti, J.M. Kenny, Carbon 43 (2005) 1499–1505.
[10] T. Liu, I.Y. Phang, L. Shen, S.Y. Chow, W.D. Zhang, Macromolecules 37 (2004) 7214–7222.
[11] R. Tenne, L. Margulis, M. Genut, G. Hodes, Nature 360 (1992) 444–446.
[12] O. Tevet, O. Goldbart, S.R. Cohen, R. Rosentsveig, R. Popovitz-Biro, H.D. Wagner, R. Tenne, Nanotechnology 21 (2010) 365705–365710.
[13] M. Naffakh, A.M. Diez-Pascual, C. Marco, M.A. Gómez, I. Jiménez, J. Phys. Chem. B 114 (2010) 11444–11453.
[14] M. Naffakh, Z. Martin, N. Fanegas, C. Marco, M.A. Gomez, I. Jiménez, J. Polym. Sci. Part B: Polym. Phys. 45 (2007) 2309–2321.
[15] L. Rapport, O. Nepomnyashchy, A. Verdyan, R. Popoviz-Biro, Y. Volovik, B. Ittah, R. Tenne, Adv. Eng. Mater. 6 (2004) 44–48.
[16] A.M. Diez-Pascual, M. Naffakh, C. Marco, G. Ellis, J. Phys. Chem. B 116 (2012) 7959–7969.
[17] A.M. Diez-Pascual, M. Naffakh, C. Marco, G. Ellis, Compos. Part A 43 (2012) 603–612.
[18] K. Nakai, T. Yokoyama, J. Solid Mech. Mater. Eng. 2 (2008) 557–566.
[19] G. Subhash, Q. Li, X.L. Gao, Int. J. Impact. Eng. 32 (2006) 1113–1126.
[20] Y. Zhou, P.K. Mallick, Polym. Eng. Sci. 42 (2002) 2449–2460.
[21] Z. Wang, Y. Zhou, P.K. Mallick, Polym. Compos. 23 (2002) 858–871.
[22] S.P. Bao, S.C. Tjong, Mater. Sci. Eng. A 485 (2008) 508–516.
[23] M.F. Omar, H.M. Akil, Z.A. Ahmad, Polym. Compos. 32 (2011) 565–575.
[24] M. Moniruzzaman, K.I. Winey, Macromolecules 39 (2006) 5194–5205.
[25] H. Krenchel, Fibre Reinforcement, Akademisk Forlag, Copenhagen, 1964.
[26] S. Deschanel, B. Greviskes, K. Bertoldi, S. Sarva, W. Chen, S. Samuels, R. Cohen, M. Boyce, Polymer 50 (2009) 227–235.
[27] T. Ree, H. Eyring, J. Appl. Phys. 26 (1955) 793–809.
[28] J.X. Li, W.L. Cheung, Polymer 39 (1998) 6935–6940.
[29] U.A. Handge, K. Hedicke-Höchstötter, V. Altstädt, Polymer 51 (2010) 2690–2699.
[30] R.-J. Zhou, T. Burkhart, J. Mater. Sci. 46 (2011) 1228–1238.
[31] I.-Y. Jeon, J.-B. Baek, Materials 3 (2010) 3654–3674.
[32] P.J. Yoon, T.D. Fornes, D.R. Paul, Polymer 43 (2002) 6727–6741.
[33] K. Kalaitzidou, H. Fukushima, L.T. Drzal, Carbon 45 (2007) 1446–1452.
[34] Y. Kojima, A. Usuki, M. Kawasumi, A. Okada, Y. Fukushima, T. Kirauchi, J. Mater. Res. 8 (1993) 1185–1189.
[35] C.A. Hieber, Polym. Eng. Sci. 42 (2002) 1387–1409.
[36] Z. Han, A. Fina, Prog. Polym. Sci. 36 (2011) 914–944.
[37] A.M. Diez-Pascual, M. Naffakh, M.A. Gómez-Fatou, Mater. Chem. Phys. 130 (2011) 126–133.
[38] T. Kashiwagi, E. Grulke, J. Hilding, K. Groth, R. Harris, K. Butler, J. Shields, S. Kharchenko, J. Douglas, Polymer 45 (2004) 4227–4239.
[39] J.C. Maxwell, A Treatise on Elec. and Magnetism, third ed,, Dover, New York, 1954.
[40] A.B. Morgan, T. Kashiwagi, R.H. Harris, J.R. Campbell, K. Shibayama, K. Iwasa, J.W. Gilman, Fire and polymers, in: G.L. Nelson, C.A. Wilkie (Eds.), ACS Symposium Series, 2001, p. 797. (Chapter 2).